

JGR Atmospheres

RESEARCH ARTICLE

10.1029/2020JD033140

Key Points:

- We investigate links between El Niño Southern Oscillation (ENSO) and East Antarctic sea ice concentration over the satellite era
- Summer/autumn sea ice concentration around Dronning Maud Land is correlated with ENSO variability
- Dronning Maud Land sea ice is linked to tropical sea surface temperature anomalies via an atmospheric wave train

Correspondence to:

F. E. Isaacs,
florence.isaacs@vuw.ac.nz

Citation:

Isaacs, F. E., Renwick, J. A., Mackintosh, A. N., & Dadic, R. (2021). ENSO modulates summer and autumn sea ice variability around Dronning Maud Land, Antarctica. *Journal of Geophysical Research: Atmospheres*, 126, e2020JD033140. <https://doi.org/10.1029/2020JD033140>

Received 27 MAY 2020
Accepted 1 FEB 2021

ENSO Modulates Summer and Autumn Sea Ice Variability Around Dronning Maud Land, Antarctica

Florence E. Isaacs¹ , James A. Renwick¹ , Andrew N. Mackintosh², and Ruzica Dadic¹ 

¹Antarctic Research Centre, School of Geography, Environment, and Earth Science, Victoria University of Wellington, Wellington, New Zealand, ²School of Earth, Atmosphere, and Environment, Monash University, Melbourne, VIC, Australia

Abstract Antarctica's sea ice cover is an important component of the global climate system, yet the drivers of sea ice variability are not well understood. Here we investigated the effects of climate variability on sea ice concentration (SIC) around East Antarctica by correlating the 40-years (1979–2018) satellite sea ice record and ERA5 reanalysis data. We found that summer and autumn SIC around Dronning Maud Land (DML) between 10 and 70°E exhibited a statistically significant negative correlation with the Niño 3.4 index. Sea ice in DML was also correlated with sea surface temperature (SST) anomalies in the tropical Pacific, and to an atmospheric wave train pattern extending from the South Pacific to DML. We suggest that a southward-propagating atmospheric wave train triggered by SST anomalies in the tropical Pacific extends into DML and alters sea ice concentration by encouraging meridional airflow. Our results showed that shifts in meridional flow in DML affected sea ice thermodynamically, by altering local heat transport and in turn altering sea ice formation and melt.

Plain Language Summary Changes in Antarctic sea ice can have a big impact on global climate. Understanding sea ice change is therefore important if we are to understand and predict future climate change. However, there is a lot of uncertainty around what controls sea ice variability. Our study investigated the links between a large-scale pattern of climate variability, El Niño Southern Oscillation (ENSO) and sea ice concentration around East Antarctica. We did so by correlating satellite records of sea ice concentration with the Niño 3.4 index (an index of ENSO activity), and modeled climate data extending from 1979 to 2018. We found that ENSO was linked to sea ice change in the Dronning Maud Land region of East Antarctica, where an El Niño phase resulted in less sea ice, and a La Niña phase resulted in more. Our findings highlight the importance of tropical variability in driving changes in Antarctic sea ice.

1. Introduction

Antarctic sea ice is an important component of the global climate system, modulating global circulation through changes to heat and moisture fluxes (Grotzner et al., 1996; Rind et al., 1995; Walsh, 1983), surface albedo (Curry et al., 1995), and production of deep ocean waters (Ferrari et al., 2014; Jacobs, 2004). Changes in sea ice distribution therefore have far-reaching consequences, and are critically important to understand in the context of broader earth-atmosphere system change. However, coupled sea-ice-climate models are currently unable to replicate current sea ice trends and variability in the Southern Ocean, predicting a negative trend where observations show a positive one (e.g., Comiso & Nishio, 2008; Polvani & Smith, 2013; Turner et al., 2013) highlighting the limitations in our understanding of the processes that drive sea ice change.

Several studies have suggested that climate variability and tropical teleconnections such as those associated with El Niño Southern Oscillation (ENSO) may play a role in determining recent sea ice variability and trends (e.g., Meehl et al., 2016; Purich et al., 2016; Raphael & Hobbs, 2014; Simmonds & Jacka, 1995; Simpkins et al., 2012; Yuan & Li, 2008). ENSO is a pattern of large-scale atmospheric and oceanic variability manifesting most prominently in a dipole in tropical Pacific SST anomalies and the perturbation of tropical convection. Changes in the tropical atmospheric circulation then propagate further into the global circulation, driving variability in precipitation (e.g., Barlow et al., 2001; Dai & Wigley, 2000; Ropelewski & Halpert, 1986), air temperatures (e.g., Power et al., 1999; Pozo-Vazquez et al., 2001; Smith & Sardeshmukh, 2000),

local winds (e.g., Romero-Centeno et al., 2003), and storm activity (e.g., Camargo & Sobel, 2005; Wang & Chan, 2002).

The influence of ENSO extends to Antarctica, affecting regional circulation (e.g., Bromwich et al., 2004; Harangozo, 2004; Schneider et al., 2012; Turner, 2004), air temperature (e.g., Q. H. Ding et al., 2011; Q. Ding & Steig, 2013; Kwok & Comiso, 2002), and precipitation (e.g., Bromwich et al., 2000; Cullather et al., 1996; Genthon & Cosme, 2003; Noone et al., 1999). The influence of ENSO is shown to affect sea ice formation, melt, and transport, leading to some covariability between ENSO and sea ice concentration (Kwok & Comiso, 2002; Liu et al., 2002; Renwick, 2002; Yuan, 2004). This signal has been identified in sea ice around West Antarctica, most prominently in the Ross, Bellingshausen, Amundsen, and Weddell Seas (e.g., Kwok et al., 2016; Simmonds & Jacka, 1995; Simpkins et al., 2012; Yuan & Li, 2008).

In East Antarctica, an ENSO signal has been identified in other components of the climate and cryosphere, including ice sheet accumulation (Boening et al., 2012), precipitation (Schlosser et al., 2010), air temperature (Schneider et al., 2012; Welhouse et al., 2016) and landfast ice (Aoki, 2017). Raphael and Hobbs (2014) and Stammerjohn et al. (2008) examined the broad links between climate variability and the sea ice advance and retreat cycle, which included sea ice averaged across East Antarctica. However, there has been little direct research into the role that ENSO and other large-scale modes of climate variability play in influencing sea ice concentration (SIC) around East Antarctica.

Our research aim was to bridge this gap by investigating the role of ENSO in influencing the past 4 decades of sea ice variability around East Antarctica. We approached this by correlating the satellite sea ice record with atmospheric reanalysis data over 1979–2018 and the Niño 3.4 ENSO index, and with composite analysis of atmospheric circulation during periods of high and low SIC. Our study focused on the region south of 50°S and between 10°E and 70°E, encompassing part of Dronning Maud Land (DML) and Enderby Land (Figure 1a).

2. Methods

2.1. Data

ENSO activity over the period 1979–2018 was examined using the ESRL/NOAA Niño 3.4 index (https://psl.noaa.gov/geos_wgsp/Timeseries/Nino34/), which is an average of sea surface temperature (SST) anomalies in the region 5°N–5°S, 170°W–120°W. The index uses monthly average temperature anomalies sourced from the National Oceanic and Atmospheric Administration (NOAA), calculated using the HadISST1 SST data set (Rayner et al., 2003) with a 1981–2010 climatological base period.

This study used the latest iteration of reanalysis from the European Center for Medium-Range Weather Forecasts (ECMWF), ERA 5 (Copernicus Climate Change Service (C3S), 2017), spanning the period from 1979 to 2018. ERA 5 is an updated version of ERA-Interim, widely regarded as the most reliable representation of the climate for the Antarctic region (Bracegirdle & Marshall, 2012). The variables examined were SST, 2 m air temperature (T2M), 500 hPa geopotential height (H500), and the vertically integrated horizontal rate of northward heat transport (NthHF), all as monthly means. As with any model product these data are not without uncertainties, but ERA5 has been shown to perform well for Antarctica, with a smaller bias relative to observations than many other reanalysis products (Gossart et al., 2019; Jones & Lister, 2015), and the coverage is substantially better than the sparse observational records that are available in the Antarctic.

Sea ice variability in this study was determined using monthly mean sea ice concentration obtained from the Met Office Hadley Center Sea Ice and SST data set (HadISST.2.2.0.0; Titchner & Rayner, 2014), comprising sea ice concentration (SIC) on a $1^\circ \times 1^\circ$ latitude-longitude grid. HadISST2 SIC is derived from satellite observations, and is one of a few complete observation-derived records of sea ice for the period from 1979 to present (National Center for Atmospheric Research Staff (Eds), 2019). In this study we used area-averaged SIC, though initial analysis suggested that it would also be possible to use the parameters of sea ice area (SIA) or sea ice extent (SIE), as they were perfectly (SIA) or highly (SIE) correlated with the averaged SIC, and showed no significant difference when correlated with ERA5 reanalysis climate fields.

Sea ice motion data were obtained from the National Snow and Ice Data Center (NSIDC), using the Polar Pathfinder Daily 25 km EASE-Grid Sea Ice Motion Vectors (Version 4) data set (Tschudi et al., 2019). Daily

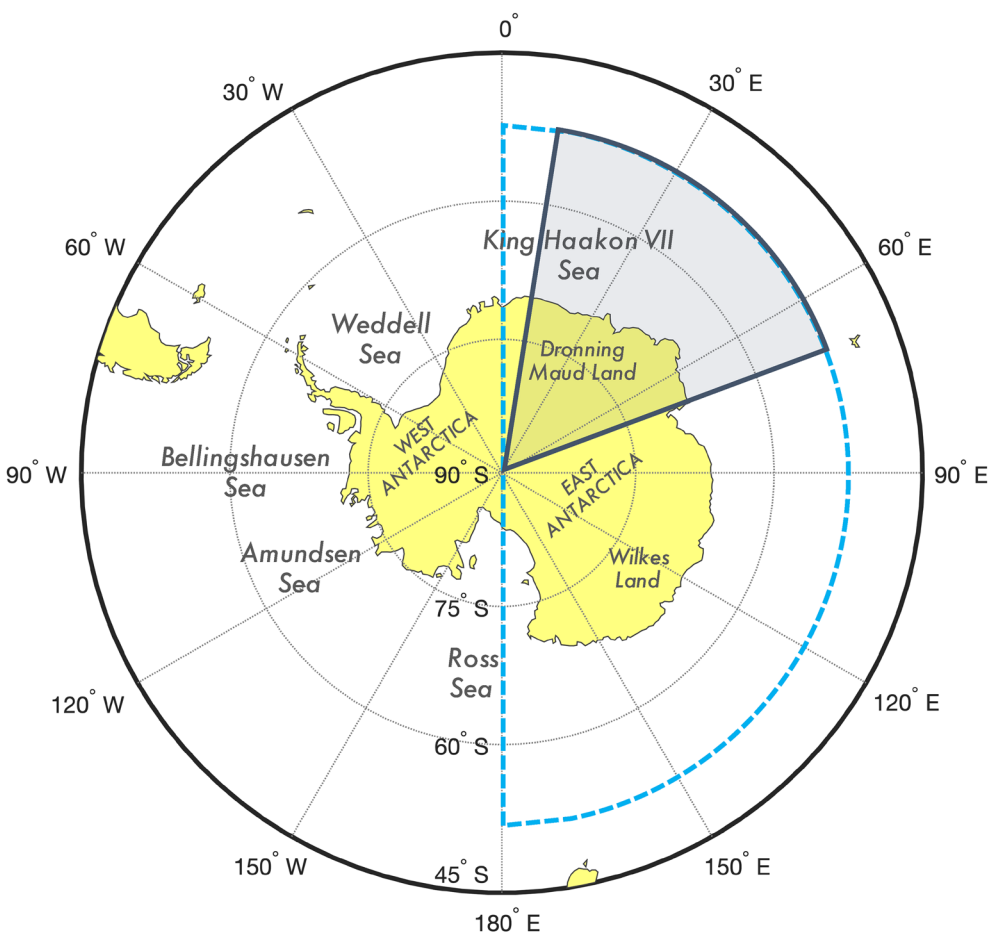


Figure 1. (a) Map of the study area including key locations discussed, and with the Dronning Maud Land/Enderby Land sector of interest (south of 50°S and between 10°E and 70°E) shaded in gray. Blue dashed line encloses the broader East Antarctic sea ice area examined.

average sea ice motion vectors were transferred from the original 25 km EASE Grid onto the same $1^\circ \times 1^\circ$ latitude-longitude grid used for the reanalysis and sea ice concentration data.

The date range for all data used in this study were 1979–2018, which marks the modern satellite era, where gridded sea ice concentration data is available and reanalysis products are reliable (Bracegirdle & Marshall, 2012).

2.2. Data Analysis

For the initial correlation analysis, gridded SIC was area-weighted and then averaged over latitudes south of 50°S, and in 10° sliding sectors of longitude between 0°E and 180°E around the coast of East Antarctica. Each sea ice sector was correlated with the Niño 3.4 index. Areas of interest were identified from this initial analysis, and SIC in the sectors between 10°E and 70°E (Dronning Maud Land/Enderby Land) was averaged and correlated against gridded H500, T2M, and SST. Each of these climate variables, along with NthHF and sea ice motion anomalies, were also correlated with the Niño 3.4 index. For wind and sea ice motion, both the U and V component of each variable were individually correlated with average SIC and the Niño 3.4 index and then plotted together as vectors, which captured the general sea ice motion/wind direction associated with SIC and Niño 3.4 anomalies.

Statistical significance of correlations was determined using a two-tailed Student's T-test, chosen due to the normal distribution of the data, with a significance level of 5% used throughout the study. SIC, H500, T2M,

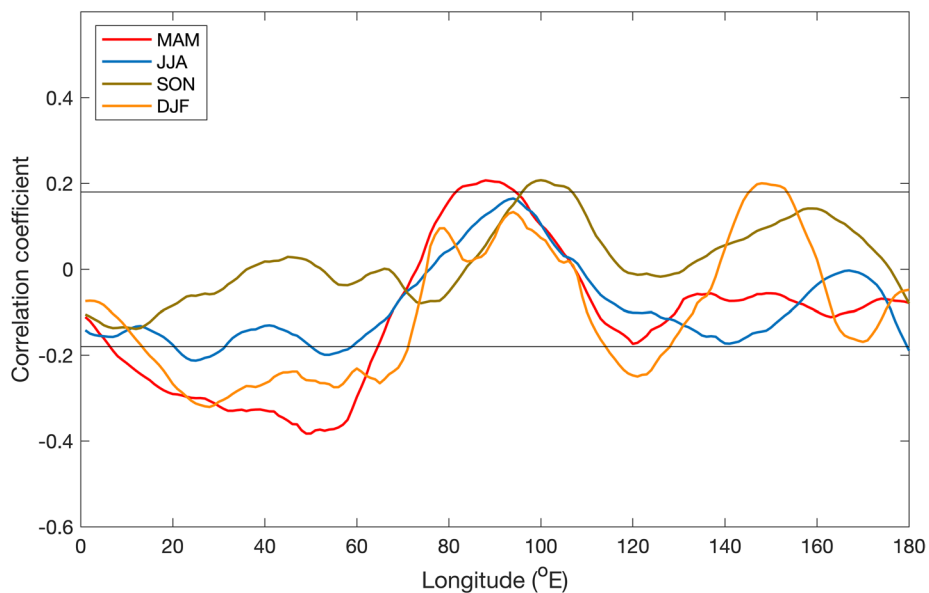


Figure 2. Correlation between Niño 3.4 index and average seasonal sea ice concentration in latitudes south of 50°S, and in 10° sliding sectors of longitude (each data point marks the start of a sector) between 0 and 180°E around the coast of East Antarctica over 1979–2018. Horizontal black lines mark statistical significance at the 5% level.

SST, and NthHF anomalies were calculated from a 1981–2010 climatological base period, removing the seasonal cycle. Seasonal averages were calculated according to austral autumn (March-April-May), winter (June-July-August), spring (September-October-November), and summer (December-January-February). The year for each summer mean was the December year. Anomaly composites examined average H500, T2M, SST, NthHF, and sea ice motion anomalies from periods when SIC in the Dronning Maud Land sector was in its upper and lower quartile (30 months for each seasonal composite), to examine nonlinearity in the response of sea ice to variability in each of these climate variables.

3. Results

Correlation analysis showed that the most significant association between the Niño 3.4 index and SIC around East Antarctica occurred in the region of Dronning Maud Land and Enderby Land between 10°E and 70°E (Figure 2). In this region, Niño 3.4 and both summer (DJF) and autumn (MAM) SIC were moderately and negatively correlated (on average $r = -0.25$ in DJF and $r = -0.38$ in MAM, $p < 0.05$). The correlation was strongest in autumn, reaching a peak of -0.38 at around 55°E (Figure 2). Other weak but statistically significant correlations between Niño 3.4 and SIC occurred in isolated regions along the rest of the East Antarctic coastline; positive correlations with SIC around 80°E–95°E (autumn), 95°E–110°E (spring), and 145°E–155°E (summer), and a negative correlation from 110°E to 130°E (summer).

In the region around DML where sea ice was significantly correlated with ENSO, the sea ice zone demonstrated substantial seasonal and interannual variability. Figure 3 shows average seasonal SIC in the region between 0 and 90°E over the period 1979–2018. Sea ice concentration around the Dronning Maud Land/Enderby Land region was highest and most spatially extensive in JJA and SON (Figures 3c and 3d), when SIC was > 0.8 from the coastline to $\sim 60^{\circ}$ S and > 0.15 (the commonly used threshold of sea ice presence/absence) to 55°S in some places. In contrast, sea ice concentrations were greater than 0.15 in MAM and DJF only in a narrow band around the coastline, extending northward by 1 or 2° (Figures 3b and 3e). SIC in the DML region also demonstrated substantial interannual variability, as shown in Figure 3a. Interannual variability was strongest in JJA and SON. The strongest positive (0.09) and negative (-0.07) SIC anomalies occurred in SON, in 2011 and 1997 respectively. In MAM and DJF (the seasons in which SIC was most strongly correlated to ENSO), interannual variability was more subdued, with the highest SIC anomaly occurring in 2011 (0.05) and the lowest in 1987 (-0.02).

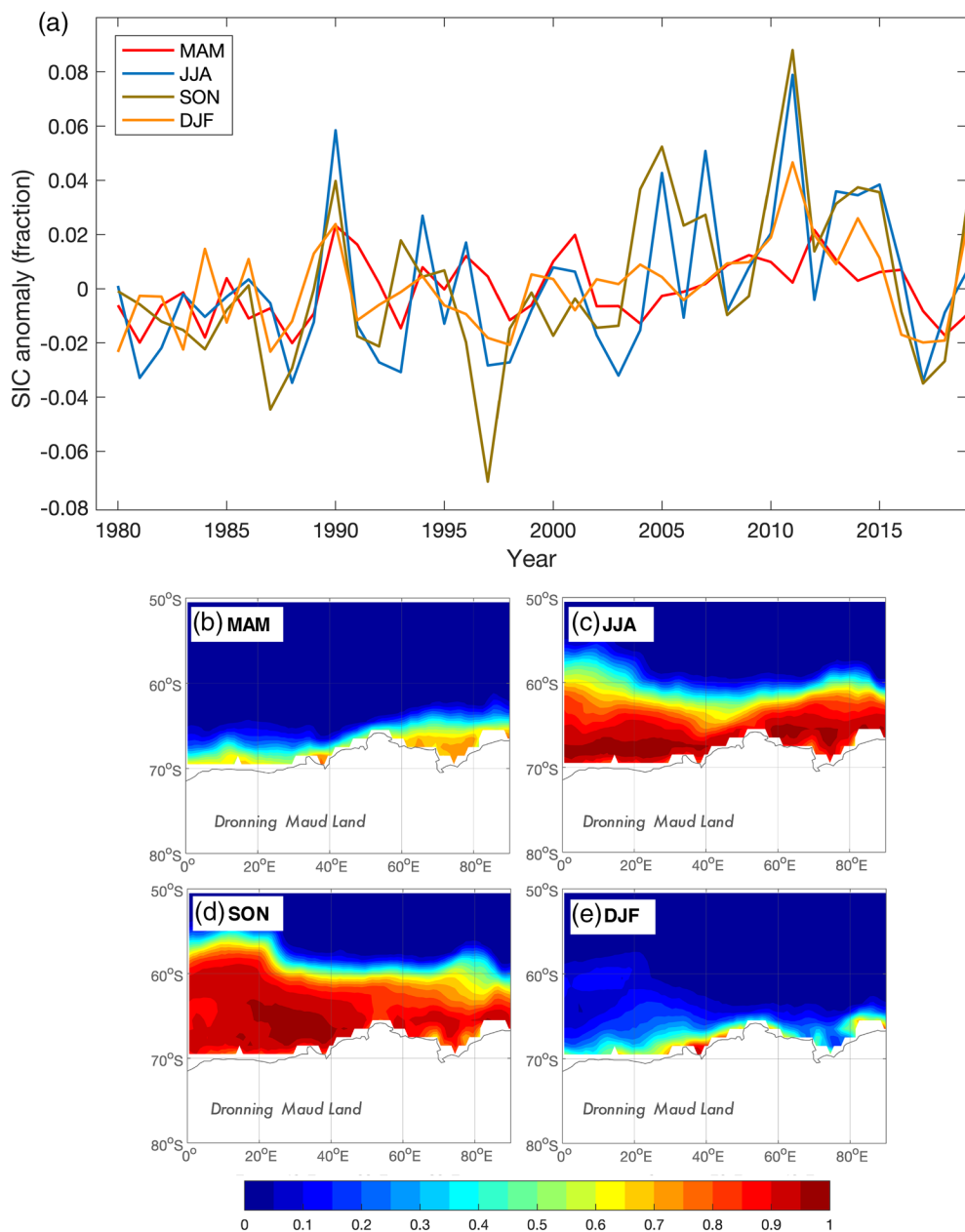


Figure 3. (a) Timeseries of seasonal HadISST sea ice concentration anomaly averaged over the Dronning Maud Land/Enderby Land sector of interest (south of 50°S and between 10 and 70°E) for the 40-year period 1979–2018; and (b–e) average seasonal HadISST sea ice concentration around the coast of Dronning Maud Land and Enderby Land, for the same time period, and where the seasons are MAM (b), JJA (c), SON (d), and DJF (e). DJF, summer; MAM, autumn.

SIC in DML was also significantly correlated with aspects of both local-scale climate around DML, and larger-scale Southern Hemisphere circulation. SIC in DML was inversely correlated with localized T2M and SST in all seasons (Figures 4 and 5), and positively correlated with a pattern of H500 consistent with anomalously southerly airflow over DML in all seasons but DJF. This pattern consisted of a positive correlation with H500 to the west of the DML region, and an inverse correlation with H500 to the east (Figure 4). All correlations were strongest and most extensive in MAM (maximum correlation magnitudes of $r = -0.7, 0.3$, and -0.6 for T2M, H500 and SST, respectively).

At a broader scale, Figures 4 and 5 also show the presence of a second center of negative correlation between DML SIC and SST or T2M in all seasons (though strongest in autumn), centered on the opposite side

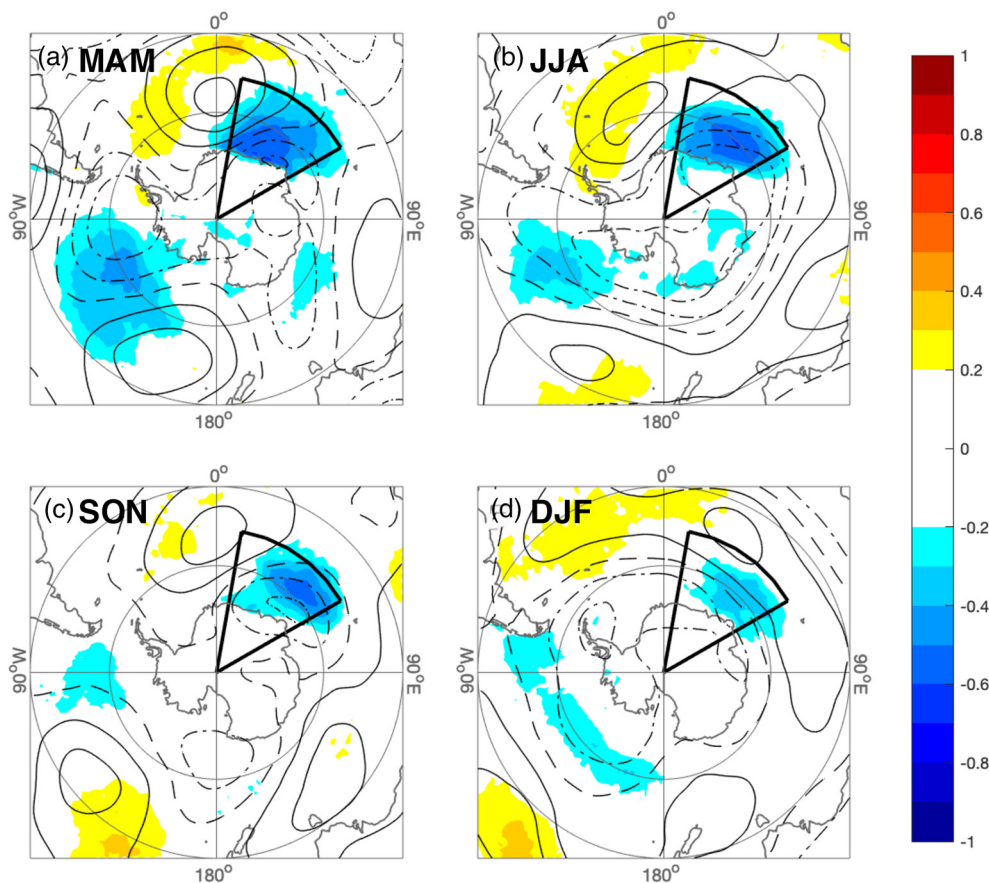


Figure 4. Correlation between SIC averaged around Dronning Maud Land (10°E – 70°E , south of 50°S , area outlined in black) with T2M (shading) and H500 (contour lines, where solid lines show positive correlation coefficients, dash-dot lines show negative, and dashed line indicates zero contour, all with contour intervals of 0.1) during MAM (a), JJA (b), SON (c), DJF (d). All T2M correlations shown are significant at the 5% level. SIC, sea ice concentration; T2M, 2 m air temperature.

of the continent to DML in the Amundsen Sea region (reaching $r = 0.5$ for SST and T2M). There was also a significant correlation between SIC in Dronning Maud Land and a distinct wave train in the H500 field (Figures 4a and 4b), linking DML to the Amundsen Sea during autumn and winter. This consisted of a positive correlation around 0°E (reaching $r = 0.4$), a negative correlation in the Amundsen Sea region (reaching $r = -0.3$), and a positive correlation north of the Ross Sea region (reaching $r = 0.3$). In areas where DML SIC was positively correlated with a pattern of H500 that would be conducive to equatorward air flow (i.e., high pressure to the west, low pressure to the east), SIC was also inversely correlated with air temperature (Figure 4), and vice versa. Figure 4 also shows evidence of a Southern Annular Mode (SAM)-like pattern in the H500 fields in JJA and most prominently in DJF, where SIC is inversely correlated to H500 over the continent, and positively correlated to H500 around the continent.

In addition to the correlations in the Southern Ocean, Figure 5 also showed a moderate inverse correlation between autumn and summer SIC in Dronning Maud Land and SST in the equatorial Pacific Ocean. The correlation was strongest and most spatially extensive in summer ($r = -0.47$), extending across the equatorial Pacific Ocean just south of the equator, from 180°E to the coast of South America (Figure 5). In SON and JJA there was only a weak negative correlation with equatorial Pacific SST covering a much smaller region than in autumn and summer (Figures 5b and 5c).

Anomaly composites of SST during periods when sea ice concentration was in the upper or lower quartile again showed links to the equatorial Pacific Ocean (Figure 6), though also revealed a degree of asymmetry in this relationship. When sea ice was particularly low in DML during autumn and summer, SST in the

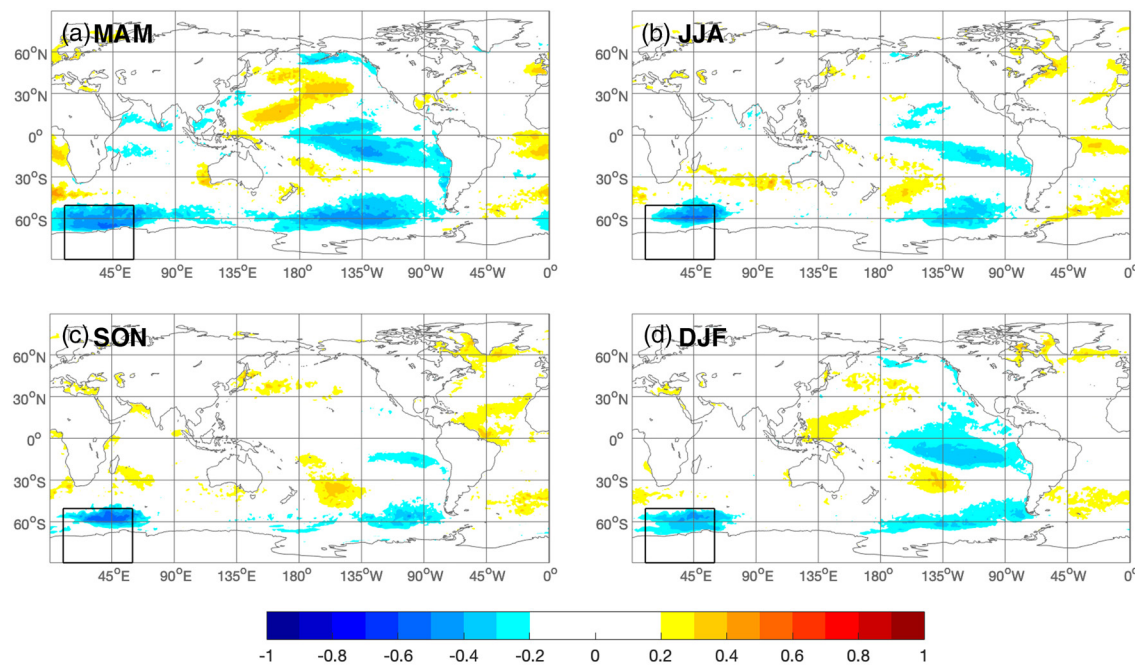


Figure 5. Correlation between SIC around Dronning Maud Land (10°E – 70°E , south of 50°S , area outlined in black) and SST during MAM (a), JJA (b), SON (c), DJF (d). All correlations shown are significant at the 5% level. SIC, sea ice concentration; SST, SST.

equatorial Pacific Ocean and off the coast of equatorial South America showed a positive anomaly of up to 0.6°C (Figures 6b and 6h). While this relationship was fairly symmetrical during DJF, it was markedly asymmetrical during MAM, with SST anomalies much weaker (between 0.1°C and 0.4°C) when SIC was in the upper quartile compared to the lower quartile. Figure 6 additionally showed stronger SST anomalies in all seasons in the DML and Amundsen/Bellingshausen sea regions when DML SIC was in the upper quartile compared to the lower quartile.

In Figures 7a and 6a, the anomaly composites of H500 during periods of higher than usual autumn SIC in DML showed the same wave train as is visible in the correlations in Figure 4 (namely a high pressure anomaly northeast of the Weddell Sea, a low pressure anomaly in the Amundsen Sea, and a high pressure anomaly north of the Ross Sea), but the composites of low SIC do so only to a much weaker extent (Figures 7e and 6b). These patterns were accompanied by anomalously high T2M over DML and over the Ross Sea ($+2^{\circ}\text{C}$) when SIC was low, and smaller negative anomalies in T2M ($<-1.0^{\circ}\text{C}$) in the Amundsen Sea, along with in DML itself (-2.5°C) when SIC is high. In DJF (Figures 7d and 7h), there were no substantial T2M anomalies when SIC was particularly high or low.

To more closely examine the mechanisms by which SIC in DML is affected by large-scale climate variability, average northward heat flux and average sea ice motion during periods when sea ice in DML was in the upper and lower quartiles of concentration were also examined. Figures 8a–8d shows a strong positive northward heat flux anomaly (i.e., increased northward transport of heat) in the western half of the DML study area when SIC in DML was particularly high, in all seasons but DJF (reaching $4 \times 10^9 \text{ W m}^{-2}$ in JJA and SON, and $2.5 \times 10^9 \text{ W m}^{-2}$ in MAM). When SIC in DML was particularly low, however, the reverse of this pattern was not reflected to the same magnitude. Smaller negative northward heat flux anomalies ($-2.5 \times 10^9 \text{ W m}^{-2}$ in MAM and SON, and $-2 \times 10^9 \text{ W m}^{-2}$ in JJA) were present in all seasons but DJF (Figures 8e–8h), though in JJA the anomalies were present in the eastern half of the DML study area rather than the west.

Sea ice motion anomalies during periods of both high and low SIC were strongest in the western half of the DML study area, between 10°E and 40°E (Figure 9). When SIC in DML was particularly high, sea ice motion in this zone exhibited a consistent eastward anomaly, particularly toward the outer edge of the sea ice (Figures 9a, 9c, 9g, and 9e). This pattern was most prominent in JJA and SON. When SIC in DML was

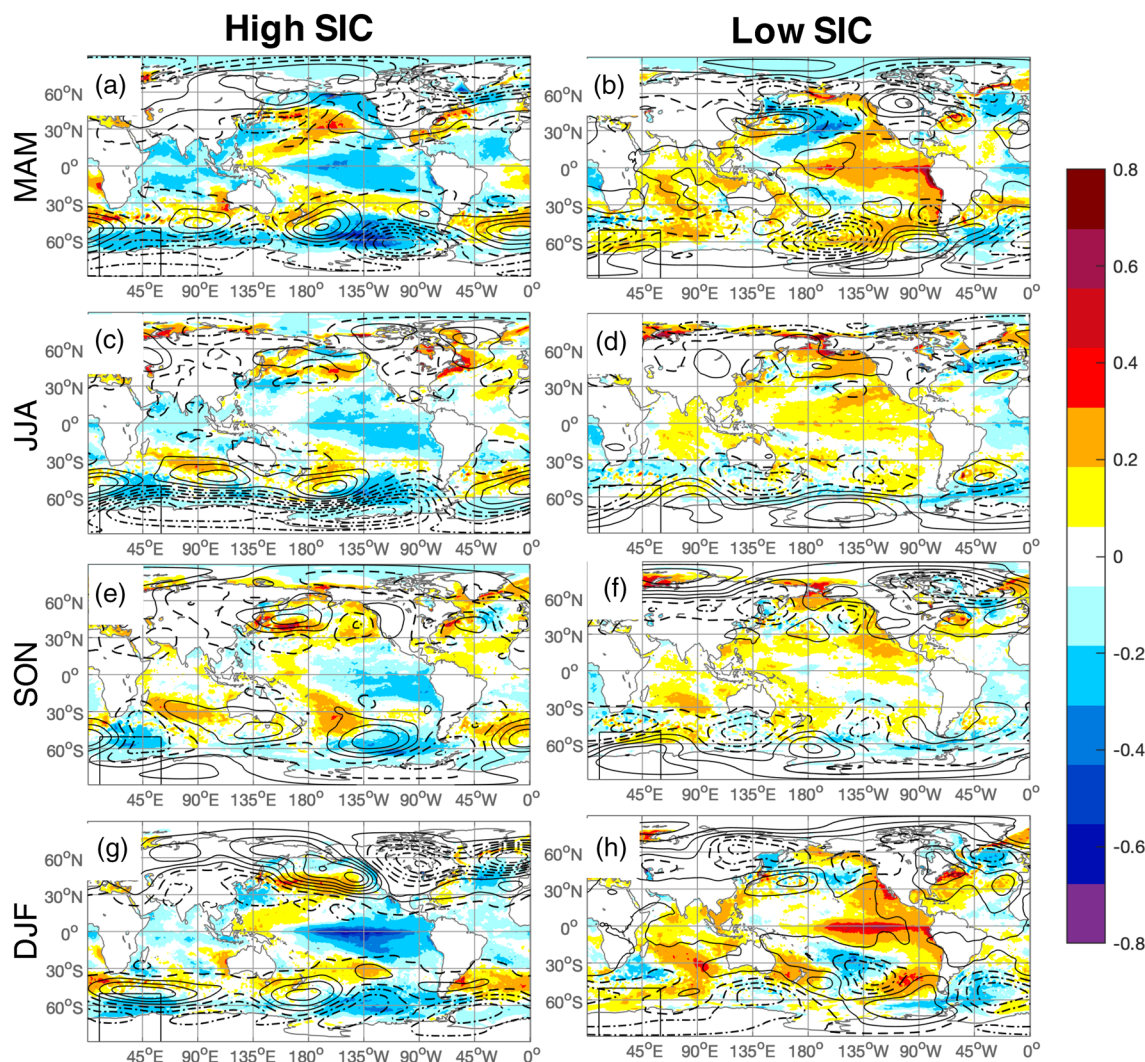


Figure 6. Anomaly composite mean for the upper (High SIC; a,c,e,g) and lower (Low SIC; b,d,f,h) quartiles of SIC around Dronning Maud Land (10°E – 70°E , south of 50°S , area outlined in black) over 1979–2018. Shading is SST anomalies ($^{\circ}\text{C}$). Contour lines show 500 hPa geopotential height anomalies (m) at 50 m intervals. Solid contours are positive anomalies, dash-dot contours are negative. SIC, sea ice concentration.

particularly low, ice motion anomalies were weaker, and showed greater variability in the direction of motion (Figures 9b, 9d, 9f, and 9h). The exception to this was in DJF, where sea ice motion was anomalously westward when SIC was low, in contrast to the anomalous eastward motion when SIC was high.

In a more direct examination of the role that ENSO plays in determining SIC in DML, Figures 10–12 show the correlation between ENSO and various aspects of the regional circulation and climate around DML. Many of the patterns evident in these figures are the same as those seen in the associations between DML SIC and climate variability, particularly in the H500, SST, and T2M fields (Figures 5 and 4). In both MAM and DJF, when ENSO and SIC were most strongly linked, ENSO variability was correlated with positive T2m (Figures 10a and 10d, correlation reaching $r = 0.47$) and SST (Figures 11a and 11d, correlation reaching $r = 0.49$) anomalies centered between 20°E and 50°E , and stretching from the coastline to 50°S . These correlations were either much weaker or not visible during JJA (Figures 10b and 11b) and SON (Figures 10c and 11c), when ENSO was not significantly correlated with SIC.

In MAM ENSO was also correlated with anomalously negative H500 over the coastline to the west of DML (centered on 0°E) with an accompanying positive anomaly in northerly winds when regressed against the Niño 3.4 index and negative correlation with northward heat flux on the eastern side of this system,

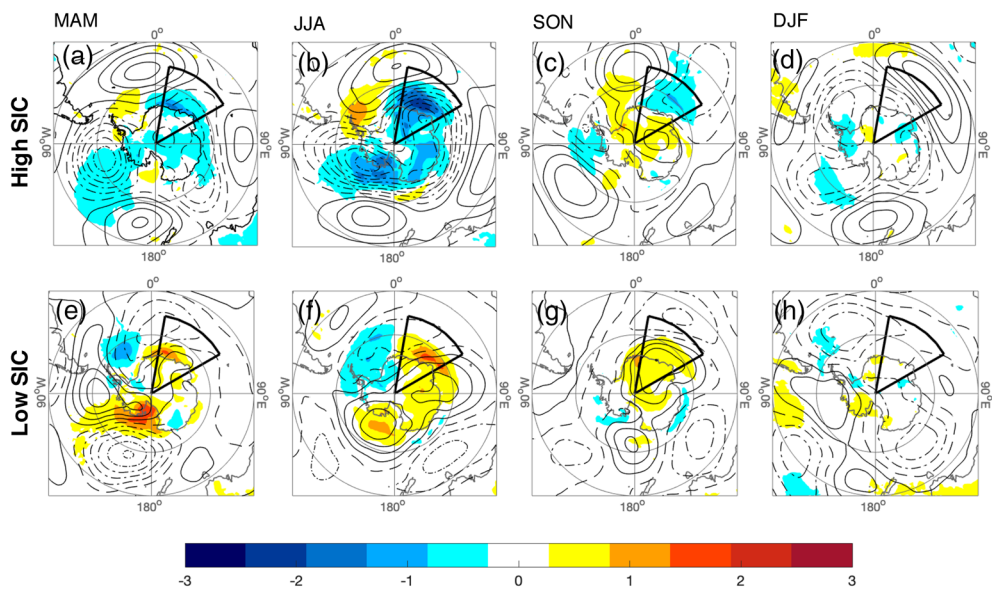
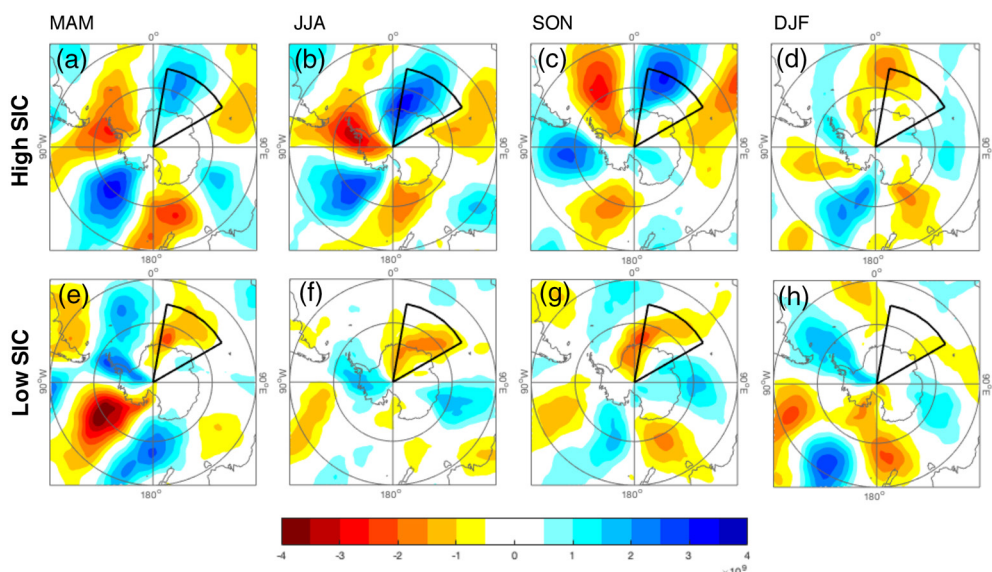


Figure 7. Anomaly composite mean for the upper (High SIC; a,b,c,d) and lower (Low SIC; e,f,g,h) quartiles of SIC around Dronning Maud Land (10°E – 70°E , south of 50°S , area outlined in black) over 1979–2018. Shading is 2 m air temperature anomalies ($^{\circ}\text{C}$). Solid contours are positive 500 hPa geopotential height anomalies (m) at 50 m intervals, dash-dot contours are negative. SIC, sea ice concentration.

extending across DML (Figures 11a and 12a). In DJF this low-pressure correlation was centered again over the meridian but further north than MAM, coupled with a positive correlation with H500 over the continent (Figures 11d). This was accompanied by increased zonal winds over the DML sea ice zone (Figure 12 south of 55°S) when regressed against the Niño 3.4 index, more northeasterly between 30°E and 60°E , and more southeasterly in all other longitudes, along with significant anomalous northwestward sea ice motion off the coast of DML (Figure 10d). In JJA and SON, when ENSO and SIC were not significantly correlated, ENSO was associated with much weaker patterns of H500 (Figures 11b and 11c) that did not match those that were correlated with DML SIC (Figures 4b and 4c).



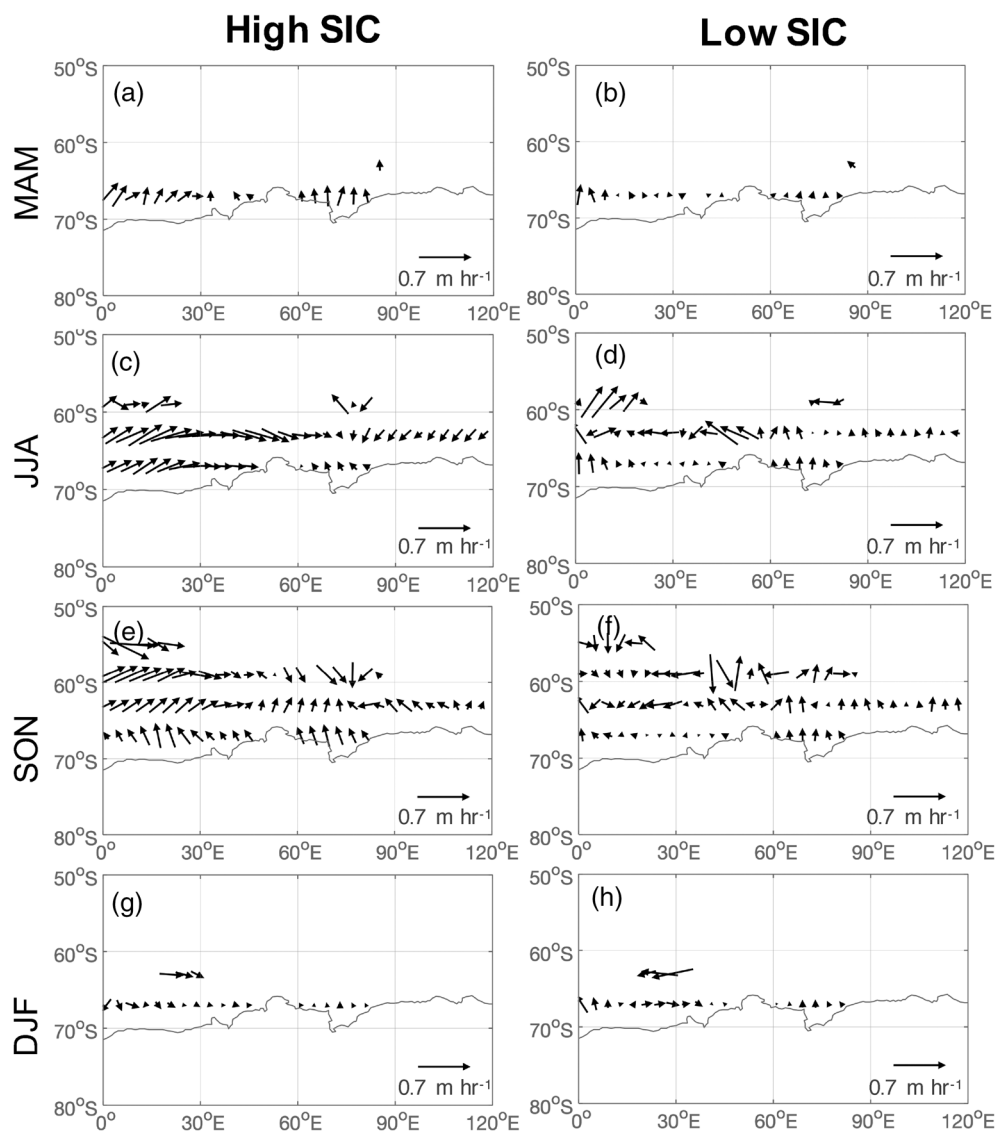


Figure 9. Anomaly composite mean sea ice motion (m h^{-1}) vectors for the upper (High SIC; a,c,e,g) and lower (Low SIC; b,d,f,h) quartiles of SIC averaged around Dronning Maud Land (10°E – 70°E , south of 50°S). Reference arrow shows a rate of 0.7 m h^{-1} .

4. Discussion

Our results show a clear statistical link between ENSO and SIC around the coast of DML and provide new insight into the role of climate variability in determining SIC in East Antarctica. There was a significant correlation between the Niño 3.4 index and sea ice concentration between 10°E and 70°E in summer and autumn, where SIC increases during a negative ENSO phase, and decreases during a positive one. Analyses of SST, T2M, and H500 fields, as discussed below, illustrate the mechanisms by which this link occurs. While past studies (e.g., Aoki, 2017; Boening et al., 2012; Noone et al., 1999) have found evidence of an ENSO signal in other aspects of the DML ice-ocean-atmosphere system, our findings extend this to include sea ice concentration, suggesting that the influence of ENSO on Antarctic sea ice is more geographically extensive than previously reported.

We suggest that ENSO exerts an influence over SIC in Dronning Maud Land through similar mechanisms as the well-established link between ENSO and sea ice in West Antarctica (e.g., in the Ross and Amundsen Seas). The West Antarctic link is driven by the perturbation of large-scale atmospheric circulation by

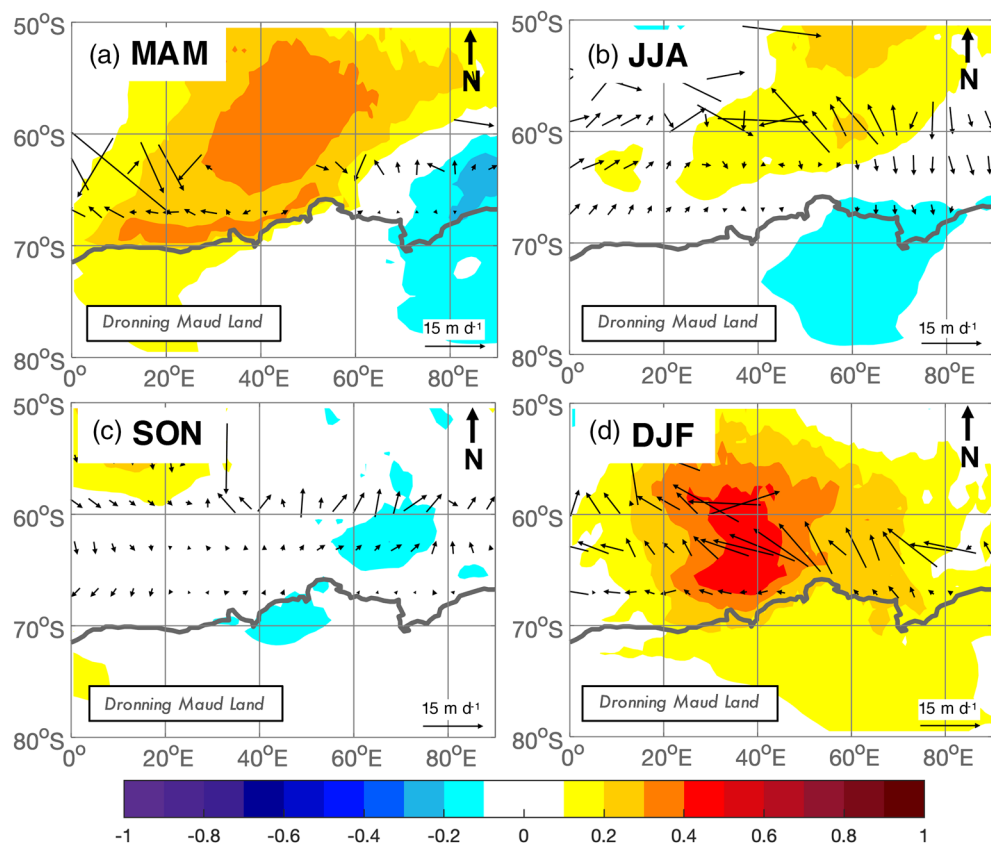


Figure 10. Correlation between the Niño 3.4 index and ERA 5 monthly average 2 m air temperature anomalies (colored shading), and regression of the NSIDC sea ice motion anomalies (vectors) against the Niño 3.4 index during MAM (a), JJA (b), SON (c), and DJF (d), across the Dronning Maud Land/Enderby Land region (0°E – 90°E). Reference arrow shows a rate of 15 m d^{-1} .

tropical Pacific SST anomalies, and the development of a southward-propagating wave train which results in low or high pressure anomalies in the Amundsen Sea region during a La Niña or El Niño respectively, and vice versa in the Weddell Sea (Kwok & Comiso, 2002; Liu et al., 2002; Yuan, 2004). These circulation changes affect local heat fluxes and advection in these regions (e.g., the Antarctic Peninsula, Amundsen/Bellingshausen Seas, and the Ross Sea), in turn influencing SIC.

We find that SIC in Dronning Maud Land was significantly correlated to SST in the Niño 3.4 region of the eastern tropical Pacific Ocean (Figures 5a–5c), and similarly to a wave train in the H500 field that extends into the south Pacific sector of the Southern Ocean, and then eastward around Antarctica (Figure 4). These patterns were also clearly visible within the SST and H500 anomalies when SIC in DML was particularly high, and to some extent when it was particularly low (Figures 6a, 6b, 6g, 6h, 7a, and 7e). The wave train appears similar to the Pacific South American pattern (PSA), a pattern of climate variability triggered by equatorial SST anomalies which is considered to be the dominant mechanism by which ENSO influences high southern latitude climates (Harangozo, 2004; Karoly, 1989; Mo & Higgins, 1998; Mo & Paegle, 2001).

The pattern in our H500 correlations (Figure 4) included a correlation with the Antarctic Dipole, a well-known feature of geopotential height and sea ice anomalies in the Amundsen and Weddell Seas (Yuan and Martinson, 2000, 2001). The dipole is driven by the PSA/ENSO, and typically consists of a negative geopotential height anomaly in the Amundsen Sea (the Amundsen Sea Low) and a positive anomaly in the Weddell Sea during La Niña, and vice versa with El Niño (Kidson & Renwick, 2002; Renwick, 2002; Yuan and Martinson, 2000, 2001). These results support the findings of Aoki (2017) and Noone et al. (1999) who suggest that the Weddell Sea component of this wave train directly affects certain aspects of the DML climate are linked to ENSO variability. Its proximity just to the west of DML means anomalous high or low

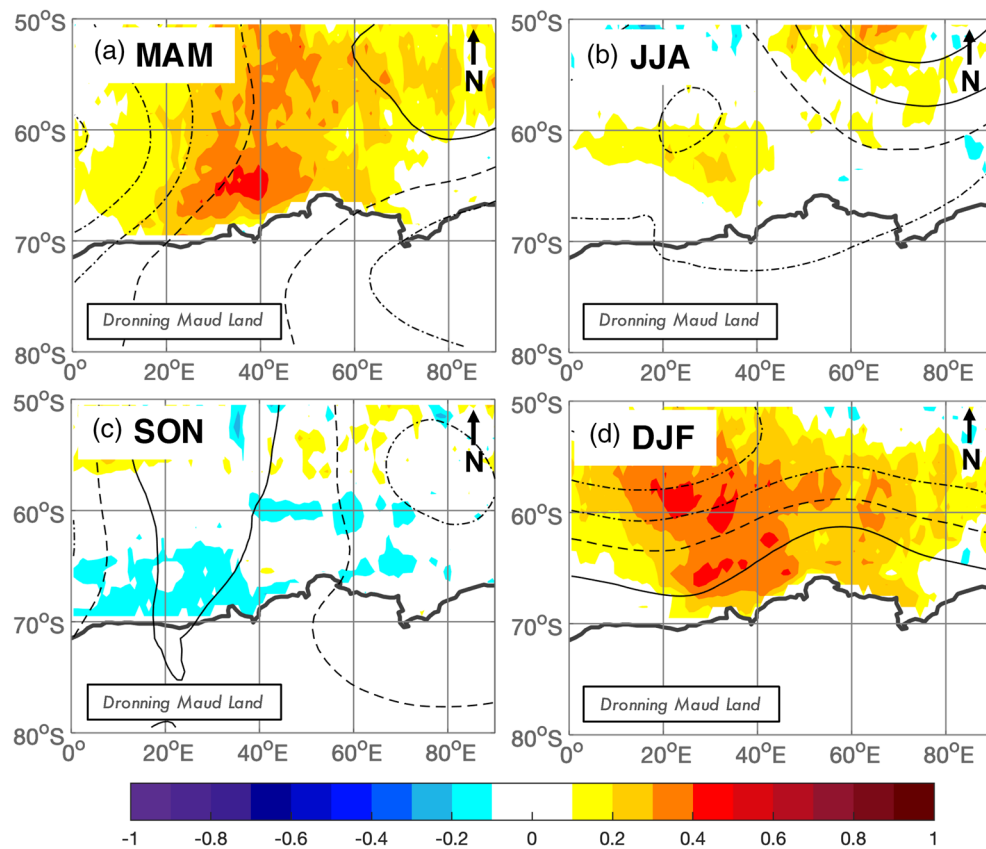


Figure 11. Correlation between the Niño 3.4 index and both ERA 5 monthly average SST anomalies (colored shading), and 500 hPa geopotential height anomalies (contour lines, where solid lines show positive correlation coefficients, dash-dot lines show negative, and dashed lines indicate zero contour, all with contour intervals of 0.1) during MAM (a), JJA (b), SON (c), and DJF (d), across the Dronning Maud Land/Enderby Land region (0°E – 90°E). SST, SST.

pressure would alter local scale wind speeds and direction, in particular the north-south airflow across DML (Hirasawa et al., 2000; Noone et al., 1999; Welhouse et al., 2016). Low pressure in the Weddell Sea (El Niño) would increase poleward (northerly) airflow across DML, while high pressure (La Niña) would increase equatorward (southerly) flow. This theory is supported by the findings in Figure 11 which show that in MAM and DJF, the H500 wave train associated with ENSO includes a center of anomalous low pressure over the meridian with the eastern limb extending over DML. Accompanying this in MAM, El Niño is associated with anomalous northerly airflow and lower than usual SIC in DML, while La Niña is associated with anomalous southerly airflow and increased SIC in DML (Figure 12).

Increased northerly airflow could be expected to drive changes in SIC through two different mechanisms. Thermodynamically, more northerly airflow would increase the advection of warm air from lower latitudes, increasing air temperature and thus increasing the surface melt of existing sea ice or decreasing the formation of new ice. Dynamically, northerly air flow would decrease transport of sea ice from the south, increasing concentration close to the coastline, but reducing overall extent (Lefebvre & Goosse, 2005; Liu et al., 2004; Turner et al., 2009). Increased southerly airflow exerts the opposite influence on sea ice for example, bringing cooler polar air over the region, and encouraging northward advection of new ice.

The covariance of the dynamic and thermodynamic impacts of meridional flow mean it is generally difficult to discern which of these mechanisms dominate. Figure 8 shows a strong association between meridional heat transport and SIC in Dronning Maud Land in all seasons but DJF, particularly when SIC is high. However, the links between SIC and sea ice motion in DML appeared to favor zonal transport over meridional transport. The association between SIC in the western side of DML and zonal sea ice motion in Figure 9, where westward transport is linked with higher SIC in all seasons, and eastward transport is additionally

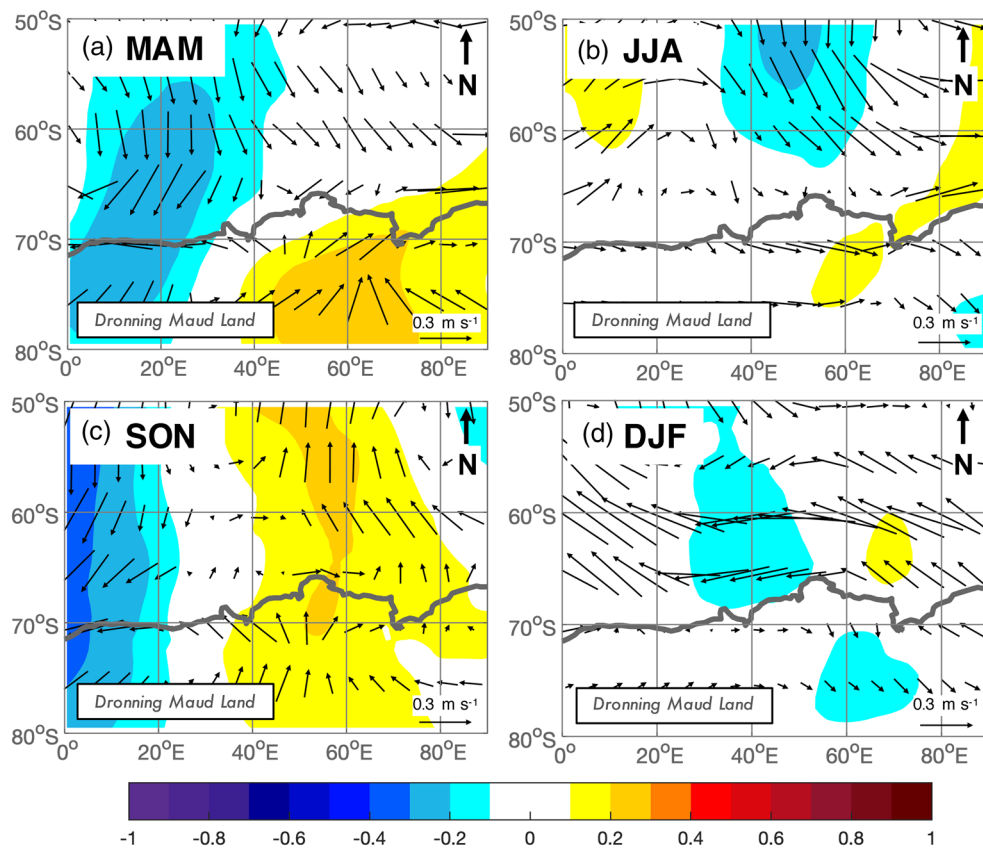


Figure 12. Correlation between the Niño 3.4 index and ERA 5 vertically integrated average northward heat flux anomalies (colored shading), and regression of 10 m wind anomalies (vectors) against the Niño 3.4 index during MAM (a), JJA (b), SON (c), and DJF (d), across the Dronning Maud Land/Enderby Land region (0°E – 90°E). Reference arrow shows a rate of 0.3 m s^{-1} .

linked with low SIC in DJF, suggests that sea ice import from the east contributes to the sea ice pack in Dronning Maud Land. This finding supports those of Kimura and Wakatsuchi (2011), who identified that SIC in the western most part of Dronning Maud Land (0°E – 30°E), is strongly contributed to by the eastward import of sea ice from the Weddell Sea.

In relation to ENSO, Figures 10–12 show that in MAM, ENSO is positively correlated with anomalous northerly winds, T2M, SST, and NthHF over the DML sea ice zone, and not substantially correlated with sea ice motion. This suggests that in MAM, the link between ENSO and SIC around DML is driven by the anomalous northward transport of heat over DML and subsequent T2M anomalies. As MAM encompasses the beginning of the sea ice growth season, these T2M anomalies would serve to either enhance (La Niña, negative T2M anomaly) or slow (El Niño, positive T2M anomaly) sea ice growth processes, driving anomalously high (La Niña) or low (El Niño) SIC around DML.

In DJF, the processes connecting DML SIC to ENSO-associated circulation anomalies appear to be different. The positive correlation with anomalous H500 centered over the meridian is much further north in DJF than in MAM. This means that ENSO is correlated with easterly and southeasterly winds over the DML sea ice zone (Figure 11), as opposed to the northerly winds associated with ENSO in MAM, and is not significantly correlated with northward heat flux. However, in DJF ENSO remains strongly correlated with SST and T2M anomalies between the coastline and 55°S , and is associated with northward sea ice transport across the DML sea ice zone.

One possible explanation is that the increased zonal component of the wind flow associated with ENSO in DJF (increased easterly winds during an El Niño and increased westerly winds during a La Niña) results in

anomalous Ekman flow (southward during El Niño, northward during La Niña), which acts to advect either warm water southward in an El Niño or cold water northward in a La Niña (Ferreira et al., 2015). As DJF is the Southern Hemisphere sea ice melt season, overall variability in SIC would be driven by variability in the amount of sea ice melt. Consequently, the warmer SST associated with an El Niño phase would then increase the rate of sea ice melt, and decrease sea ice concentration around DML. During a La Niña phase, the advection of cooler water northward would do the opposite, slowing the rate of sea ice melt and thus drive anomalously high SIC.

In addition, the positive correlation between ENSO and northeasterward sea ice motion during DJF could be explained by the influence that sea ice concentration has on sea ice motion. Higher SIC means a more consolidated sea ice pack that is more resistant to wind- or ocean-forced advection (Kimura, 2004; Steele et al., 1997). This could mean that the increased northward transport of sea ice during El Niño phases (southward transport during La Niña) that we see in Figure 10 may be a product of the anomalously low SIC (high SIC during La Niña) driven by the process described above.

In terms of the seasonality of the ENSO signal in DML, its prevalence in austral summer and autumn but not throughout the rest of the year is broadly consistent with the findings of e.g., Yuan (2004), Okumura and Deser (2010), and Pope et al. (2017). These studies identified that the teleconnection between ENSO and the Antarctic climate is at its strongest during summer (Okumura & Deser, 2010; Yuan, 2004) when ENSO activity peaks, before decaying further into winter. However, the impact of the teleconnection on sea ice has been suggested to be strongest in autumn, when sea ice is expanding (Pope et al., 2017; Yuan, 2004), explaining the strong correlation we see between DML SIC and ENSO in autumn.

One factor not investigated by this study was the covariance of ENSO with other modes of climate variability. The influence of ENSO on SIC in West Antarctica is known to work in tandem with the Southern Annular Mode (SAM), working to enhance or diminish the effects of ENSO depending on its phase (Fogt & Bromwich, 2006; L'Heureux & Thompson, 2006; Zhou & Yu, 2004). Results in Figure 4 showed evidence of a SAM-like pattern in the correlation between SIC and H500 geopotential height in JJA and DJF, suggesting some SAM influence around DML. Further research is needed to determine whether ENSO and SAM interact in this region, and work similarly as in West Antarctica to influence SIC change.

5. Conclusions

To our knowledge, our study identifies the first clear link between ENSO and SIC in East Antarctica in the Dronning Maud Land sector. Our results showed a strong negative linear correlation between satellite-derived SIC and the Niño 3.4 index in austral summer and autumn persisting between 10°E and 70°E, around the coast of Dronning Maud Land and Enderby Land. Using ERA5 reanalysis, we found that within this same region SIC is strongly correlated with tropical Pacific SST, and with a wave train in SST and H500 bearing similarity to the PSA-1 pattern, resulting in a strong correlation with H500 in the Weddell Sea. These results suggest that an atmospheric wave train triggered by ENSO SST anomalies in the Pacific alters North-South flow over DML, driving changes to local scale heat fluxes and advection, and affecting the formation, melt, and transport of sea ice in the region.

These findings underscore the importance of atmospheric circulation in determining Antarctic SIC, and suggest that the influence of ENSO on SIC is more extensive than previously thought, extending into the East Antarctic region. Further research is needed to identify the precise mechanisms by which these links occur, and how this tropical-polar teleconnection may be affected by projected climate change.

Data Availability Statement

All data used in this study are freely available online. The HadISST.2.2.0.0 sea ice concentration data can be found at (<https://www.metoffice.gov.uk/hadobs/hadisst/>), NSIDC sea ice motion vectors at (<https://nsidc.org/data/nsidc-0116>), ERA5 reanalysis at (<https://cds.climate.copernicus.eu>), and the Niño 3.4 index time-series at (https://psl.noaa.gov/gcos_wgsp/Timeseries/Nino34/).

Acknowledgments

This research was supported by funding from Antarctica New Zealand.

References

- Aoki, S. (2017). Breakup of land-fast sea ice in Lutzow-Holm Bay, East Antarctica, and its teleconnection to tropical Pacific sea surface temperatures. *Geophysical Research Letters*, 44(7), 3219–3227. <https://doi.org/10.1002/2017gl072835>
- Barlow, M., Nigam, S., & Berbery, E. H. (2001). ENSO, Pacific decadal variability, and US summertime precipitation, drought, and stream flow. *Journal of Climate*, 14(9), 2105–2128. [https://doi.org/10.1175/1520-0442\(2001\)014\(2105:Epda\)2.0.Co;2](https://doi.org/10.1175/1520-0442(2001)014(2105:Epda)2.0.Co;2)
- Boening, C., Lebsack, M., Landerer, F., & Stephens, G. (2012). Snowfall-driven mass change on the East Antarctic ice sheet. *Geophysical Research Letters*, 39, L21501. <https://doi.org/10.1029/2012gl053316>
- Bracegirdle, T. J., & Marshall, G. J. (2012). The reliability of Antarctic tropospheric pressure and temperature in the latest global reanalyses. *Journal of Climate*, 25(20), 7138–7146. <https://doi.org/10.1175/Jcli-D-11-00685.1>
- Bromwich, D. H., Monaghan, A. J., & Guo, Z. C. (2004). Modeling the ENSO modulation of Antarctic climate in the late 1990s with the polar MMS. *Journal of Climate*, 17(1), 109–132. [https://doi.org/10.1175/1520-0442\(2004\)017\(0109:Mtemoa\)2.0.Co;2](https://doi.org/10.1175/1520-0442(2004)017(0109:Mtemoa)2.0.Co;2)
- Bromwich, D. H., Rogers, A. N., Kallberg, P., Cullather, R. I., White, J. W. C., & Kreutz, K. J. (2000). ECMWF analyses and reanalyses depiction of ENSO signal in antarctic precipitation. *Journal of Climate*, 13(8), 1406–1420. [https://doi.org/10.1175/1520-0442\(2000\)013\(1406:Eaard\)2.0.Co;2](https://doi.org/10.1175/1520-0442(2000)013(1406:Eaard)2.0.Co;2)
- Camargo, S. J., & Sobel, A. H. (2005). Western North Pacific tropical cyclone intensity and ENSO. *Journal of Climate*, 18(15), 2996–3006. <https://doi.org/10.1175/Jcli3457.1>
- Comiso, J. C., & Nishio, F. (2008). Trends in the sea ice cover using enhanced and compatible AMSR-E, SSM/I, and SMMR data. *Journal of Geophysical Research*, 113(C2). <https://doi.org/10.1029/2007JC004257>
- Copernicus Climate Change Service (C3S). (2017). ERA5: Fifth generation of ECMWF atmospheric reanalyses of the global climate. Copernicus climate change Service climate data store (CDS). Retrieved from <https://cds.climate.copernicus.eu/cdsapp#!/home>
- Cullather, R. I., Bromwich, D. H., & VanWoert, M. L. (1996). Interannual variations in Antarctic precipitation related to El Niño southern oscillation. *Journal of Geophysical Research*, 101(D14), 19109–19118. <https://doi.org/10.1029/96jd01769>
- Curry, J. A., Schramm, J. L., & Ebert, E. E. (1995). Sea-ice albedo climate feedback mechanism. *Journal of Climate*, 8(2), 240–247. [https://doi.org/10.1175/1520-0442\(1995\)008\(0240:Siacf\)2.0.Co;2](https://doi.org/10.1175/1520-0442(1995)008(0240:Siacf)2.0.Co;2)
- Dai, A., & Wigley, T. M. L. (2000). Global patterns of ENSO-induced precipitation. *Geophysical Research Letters*, 27(9), 1283–1286. <https://doi.org/10.1029/1999gl011140>
- Ding, Q., & Steig, E. J. (2013). Temperature change on the Antarctic Peninsula linked to the tropical Pacific. *Journal of Climate*, 26(19), 7570–7585.
- Ding, Q. H., Steig, E. J., Battisti, D. S., & Kuttel, M. (2011). Winter warming in West Antarctica caused by central tropical Pacific warming. *Nature Geoscience*, 4(6), 398–403. <https://doi.org/10.1038/Ngeo1129>
- Ferrari, R., Jansen, M. F., Adkins, J. F., Burke, A., Stewart, A. L., & Thompson, A. F. (2014). Antarctic sea ice control on ocean circulation in present and glacial climates. *Proceedings of the National Academy of Sciences of the United States of America*, 111(24), 8753–8758. <https://doi.org/10.1073/pnas.1323922111>
- Ferreira, D., Marshall, J., Bitz, C. M., Solomon, S., & Plumb, A. (2015). Antarctic ocean and sea ice response to ozone depletion: A two-time-scale problem. *Journal of Climate*, 28(3), 1206–1226.
- Fogt, R. L., & Bromwich, D. H. (2006). Decadal variability of the ENSO teleconnection to the high-latitude South Pacific governed by coupling with the southern annular mode. *Journal of Climate*, 19(6), 979–997. <https://doi.org/10.1175/Jcli3671.1>
- Genthon, C., & Cosme, E. (2003). Intermittent signature of ENSO in west-Antarctic precipitation. *Geophysical Research Letters*, 30(21). <https://doi.org/10.1029/2003gl018280>
- Gossart, A., Helsen, S., Lenaerts, J., Broucke, S., van Lipzig, N., & Souverijns, N. (2019). An evaluation of surface climatology in state-of-the-art reanalyses over the Antarctic ice sheet. *Journal of Climate*, 32(20), 6899–6915. <https://doi.org/10.1175/JCLI-D-19-0030.1>
- Grotzner, A., Sausen, R., & Claussen, M. (1996). The impact of sub-grid scale sea-ice inhomogeneities on the performance of the atmospheric general circulation model ECHAM3. *Climate Dynamics*, 12(7), 477–496. <https://doi.org/10.1007/s003820050122>
- Harangozo, S. A. (2004). The impact of winter ice retreat on antarctic winter sea-ice extent and links to the atmospheric meridional circulation. *International Journal of Climatology*, 24(8), 1023–1044. <https://doi.org/10.1002/joc.1046>
- Hirasawa, N., Nakamura, H., & Yamanouchi, T. (2000). Abrupt changes in meteorological conditions observed at an inland Antarctic station in association with wintertime blocking. *Geophysical Research Letters*, 27(13), 1911–1914. <https://doi.org/10.1029/1999gl011039>
- Jacobs, S. S. (2004). Bottom water production and its links with the thermohaline circulation. *Antarctic Science*, 16(4), 427–437. <https://doi.org/10.1017/S095410200400224x>
- Jones, P. D., & Lister, D. H. (2015). Antarctic near-surface air temperatures compared with ERA-Interim values since 1979. *International Journal of Climatology*, 35(7), 1354–1366. <https://doi.org/10.1002/joc.4061>
- Karoly, D. J. (1989). Southern-hemisphere circulation features associated with El Niño—southern oscillation events. *Journal of Climate*, 2(11), 1239–1252. [https://doi.org/10.1175/1520-0442\(1989\)002\(1239:Shcfaw\)2.0.Co;2](https://doi.org/10.1175/1520-0442(1989)002(1239:Shcfaw)2.0.Co;2)
- Kidson, J. W., & Renwick, J. A. (2002). The southern hemisphere evolution of ENSO during 1981–99. *Journal of Climate*, 15(8), 847–863. [https://doi.org/10.1175/1520-0442\(2002\)015\(0847:Tshoe\)2.0.Co;2](https://doi.org/10.1175/1520-0442(2002)015(0847:Tshoe)2.0.Co;2)
- Kimura, N., & Wakatsuchi, M. (2011). Large-scale processes governing the seasonal variability of the Antarctic sea ice. *Tellus A: Dynamic Meteorology and Oceanography*, 63(4), 828–840.
- Kwok, R., & Comiso, J. C. (2002). Spatial patterns of variability in Antarctic surface temperature: Connections to the southern hemisphere annular mode and the southern oscillation. *Geophysical Research Letters*, 29(14), 501–504. <https://doi.org/10.1029/2002gl015415>
- Kwok, R., Comiso, J. C., Lee, T., & Holland, P. R. (2016). Linked trends in the south Pacific sea ice edge and southern oscillation index. *Geophysical Research Letters*, 43(19), 10295–10302. <https://doi.org/10.1002/2016gl070655>
- Lefebvre, W., & Goosse, H. (2005). Influence of the southern annular mode on the sea ice-ocean system: The role of the thermal and mechanical forcing. *Ocean Science*, 1(3), 145–157. <https://doi.org/10.5194/os-1-145-2005>
- L'Heureux, M. L., & Thompson, D. W. J. (2006). Observed relationships between the El Niño-Southern Oscillation and the extratropical zonal-mean circulation. *Journal of Climate*, 19(2), 276–287. <https://doi.org/10.1175/Jcli3617.1>
- Liu, J. P., Curry, J. A., & Martinson, D. G. (2004). Interpretation of recent Antarctic sea ice variability. *Geophysical Research Letters*, 31(2), L02205. <https://doi.org/10.1029/2003gl018732>
- Liu, J. P., Martinson, D. G., Yuan, X. J., & Rind, D. (2002). Evaluating Antarctic sea ice variability and its teleconnections in global climate models. *International Journal of Climatology*, 22(8), 885–900. <https://doi.org/10.1002/joc.770>
- Meehl, G. A., Arblaster, J. M., Bitz, C. M., Chung, C. T. Y., & Teng, H. Y. (2016). Antarctic sea-ice expansion between 2000 and 2014 driven by tropical Pacific decadal climate variability. *Nature Geoscience*, 9(8), 590–595. <https://doi.org/10.1038/Ngeo2751>

- Mo, K. C., & Higgins, R. W. (1998). The Pacific-South American modes and tropical convection during the Southern Hemisphere winter. *Monthly Weather Review*, 126(6), 1581–1596. [https://doi.org/10.1175/1520-0493\(1998\)126%3c1581:Tpsama%3d2.0.Co;2](https://doi.org/10.1175/1520-0493(1998)126%3c1581:Tpsama%3d2.0.Co;2)
- Mo, K. C., & Paegle, J. N. (2001). The Pacific-South American modes and their downstream effects. *International Journal of Climatology*, 21(10), 1211–1229. <https://doi.org/10.1002/joc.685>
- National Center for Atmospheric Research Staff (Eds). (2019). The climate data guide: Sea ice concentration data from HadISST. Retrieved from <https://climatedataguide.ucar.edu/climate-data/sea-ice-concentration-data-hadisst>
- Noone, D., Turner, J., & Mulvaney, R. (1999). Atmospheric signals and characteristics of accumulation in Dronning Maud Land, Antarctica. *Journal of Geophysical Research*, 104(D16), 19191–19211. <https://doi.org/10.1029/1999jd900376>
- Okumura, Y. M., & Deser, C. (2010). Asymmetry in the duration of El Niño and La Niña. *Journal of Climate*, 23(21), 5826–5843. <https://doi.org/10.1175/2010jcli3592.1>
- Polvani, L. M., & Smith, K. L. (2013). Can natural variability explain observed antarctic sea ice trends? new modeling evidence from cmip5. *Geophysical Research Letters*, 40(12), 3195–3199.
- Pope, J. O., Holland, P. R., Orr, A., Marshall, G. J., & Phillips, T. (2017). The impacts of El Niño on the observed sea ice budget of West Antarctica. *Geophysical Research Letters*, 44(12), 6200–6208. <https://doi.org/10.1002/2017gl073414>
- Power, S., Casey, T., Folland, C., Colman, A., & Mehta, V. (1999). Inter-decadal modulation of the impact of ENSO on Australia. *Climate Dynamics*, 15(5), 319–324. <https://doi.org/10.1007/s003820050284>
- Pozo-Vazquez, D., Esteban-Parra, M. J., Rodrigo, F. S., & Castro-Diez, Y. (2001). The association between ENSO and winter atmospheric circulation and temperature in the North Atlantic region. *Journal of Climate*, 14(16), 3408–3420. [https://doi.org/10.1175/1520-0442\(2001\)014%3c3408:Tabeaw%3e2.0.Co;2](https://doi.org/10.1175/1520-0442(2001)014%3c3408:Tabeaw%3e2.0.Co;2)
- Purich, A., England, M. H., Cai, W., Chikamoto, Y., Timmermann, A., Fyfe, J. C., et al. (2016). Tropical Pacific SST drivers of recent Antarctic sea ice trends. *Journal of Climate*, 29(24), 8931–8948. <https://doi.org/10.1175/Jcli-D-16-0440.1>
- Raphael, M. N., & Hobbs, W. (2014). The influence of the large-scale atmospheric circulation on Antarctic sea ice during ice advance and retreat seasons. *Geophysical Research Letters*, 41(14), 5037–5045. <https://doi.org/10.1002/2014gl060365>
- Rayner, N. A., Parker, D. E., Horton, E. B., Folland, C. K., Alexander, L. V., Rowell, D. P., et al. (2003). Global analyses of sea surface temperature, sea ice, and night marine air temperature since the late nineteenth century. *Journal of Geophysical Research*, 108(D14). <https://doi.org/10.1029/2002jd002670>
- Renwick, J. A. (2002). Southern hemisphere circulation and relations with sea ice and sea surface temperature. *Journal of Climate*, 15(21), 3058–3068. [https://doi.org/10.1175/1520-0442\(2002\)015%3c3058:Shcarw%3e2.0.Co;2](https://doi.org/10.1175/1520-0442(2002)015%3c3058:Shcarw%3e2.0.Co;2)
- Rind, D., Healy, R., Parkinson, C., & Martinson, D. (1995). The Role of sea-ice in 2X Co2 climate model sensitivity .1. The total influence of sea-ice thickness and extent. *Journal of Climate*, 8(3), 449–463. [https://doi.org/10.1175/1520-0442\(1995\)008%3c449:Tosii%3e2.0.Co;2](https://doi.org/10.1175/1520-0442(1995)008%3c449:Tosii%3e2.0.Co;2)
- Romero-Centeno, R., Zavala-Hidalgo, J., Gallegos, A., & O'Brien, J. J. (2003). Isthmus of Tehuantepec wind climatology and ENSO signal. *Journal of Climate*, 16(15), 2628–2639. [https://doi.org/10.1175/1520-0442\(2003\)016%3c2628:Iotwca%3e2.0.Co;2](https://doi.org/10.1175/1520-0442(2003)016%3c2628:Iotwca%3e2.0.Co;2)
- Ropelewski, C. F., & Halpert, M. S. (1986). North-American precipitation and temperature patterns associated with the El Niño southern oscillation (ENSO). *Monthly Weather Review*, 114(12), 2352–2362. [https://doi.org/10.1175/1520-0493\(1986\)114%3c2352:Napats%3e2.0.Co;2](https://doi.org/10.1175/1520-0493(1986)114%3c2352:Napats%3e2.0.Co;2)
- Schlosser, E., Powers, J. G., Duda, M. G., Manning, K. W., Reijmer, C. H., & van den Broeke, M. R. (2010). An extreme precipitation event in Dronning Maud Land, Antarctica: A case study with the Antarctic mesoscale prediction system. *Polar Research*, 29(3), 330–344. <https://doi.org/10.1111/j.1751-8369.2010.00164.x>
- Schneider, D. P., Okumura, Y., & Deser, C. (2012). Observed Antarctic interannual climate variability and tropical linkages. *Journal of Climate*, 25(12), 4048–4066. <https://doi.org/10.1175/Jcli-D-11-00273.1>
- Simmonds, I., & Jacka, T. H. (1995). Relationships between the interannual variability of Antarctic sea-ice and the southern oscillation. *Journal of Climate*, 8(3), 637–647. [https://doi.org/10.1175/1520-0442\(1995\)008%3c637:Rbtivo%3e2.0.Co;2](https://doi.org/10.1175/1520-0442(1995)008%3c637:Rbtivo%3e2.0.Co;2)
- Simpkins, G. R., Ciasto, L. M., Thompson, D. W. J., & England, M. H. (2012). Seasonal relationships between large-scale climate variability and Antarctic sea ice concentration. *Journal of Climate*, 25(16), 5451–5469. <https://doi.org/10.1175/Jcli-D-11-00367.1>
- Smith, C. A., & Sardeshmukh, P. D. (2000). The effect of ENSO on the intraseasonal variance of surface temperatures in winter. *International Journal of Climatology*, 20(13), 1543–1557. [https://doi.org/10.1002/1097-0088\(20001115\)20:13%3c1543::Aid-Joc579%3e3.0.Co;2-A](https://doi.org/10.1002/1097-0088(20001115)20:13%3c1543::Aid-Joc579%3e3.0.Co;2-A)
- Stammerjohn, S. E., Martinson, D. G., Smith, R. C., Yuan, X., & Rind, D. (2008). Trends in Antarctic annual sea ice retreat and advance and their relation to El Niño-southern oscillation and southern annular mode variability. *Journal of Geophysical Research*, 113(C3). <https://doi.org/10.1029/2007jc004269>
- Steele, M., Zhang, J., Rothrock, D., & Stern, H. (1997). The force balance of sea ice in a numerical model of the Arctic Ocean. *Journal of Geophysical Research: Oceans*, 102(C9), 21061–21079.
- Titchner, H. A., & Rayner, N. A. (2014). The met office Hadley centre sea ice and sea surface temperature data set, version 2: 1. Sea ice concentrations. *Journal of Geophysical Research: Atmospheres*, 119(6), 2864–2889. <https://doi.org/10.1002/2013jd020316>
- Tschudi, M., Meier, W. N., Stewart, J., Fowler, C., & Maslanik, J. (2019). *Polar pathfinder daily 25 km EASE-Grid Sea ice motion vectors (Version 4)*. Boulder, CO:NASA National Snow and Ice Data Center Distributed Active Archive Center. Retrieved from <https://doi.org/10.5067/INAWUWO7QH7B>
- Turner, J. (2004). The El Niño-southern oscillation and Antarctica. *International Journal of Climatology*, 24(1), 1–31. <https://doi.org/10.1002/joc.965>
- Turner, J., Bracegirdle, T. J., Phillips, T., Marshall, G. J., & Hosking, J. S. (2013). An initial assessment of Antarctic sea ice extent in the cmip5 models. *Journal of Climate*, 26(5), 1473–1484
- Turner, J., Comiso, J. C., Marshall, G. J., Lachlan-Cope, T. A., Bracegirdle, T., Maksym, T., et al. (2009). Non-annular atmospheric circulation change induced by stratospheric ozone depletion and its role in the recent increase of Antarctic sea ice extent. *Geophysical Research Letters*, 36. <https://doi.org/10.1029/2009gl037524>
- Walsh, J. E. (1983). The role of sea ice in climatic variability: Theories and evidence. *Atmosphere-Ocean*, 21(3), 229–242
- Wang, B., & Chan, J. C. L. (2002). How strong ENSO events affect tropical storm activity over the Western North Pacific. *Journal of Climate*, 15(13), 1643–1658. [https://doi.org/10.1175/1520-0442\(2002\)015%3c1643:Hseeat%3d2.0.Co;2](https://doi.org/10.1175/1520-0442(2002)015%3c1643:Hseeat%3d2.0.Co;2)
- Welhouse, L. J., Lazzara, M. A., Keller, L. M., Tripoli, G. J., & Hitchman, M. H. (2016). Composite analysis of the effects of ENSO events on Antarctica. *Journal of Climate*, 29(5), 1797–1808. <https://doi.org/10.1175/Jcli-D-15-0108.1>
- Yuan, X. J. (2004). ENSO-related impacts on Antarctic sea ice: a synthesis of phenomenon and mechanisms. *Antarctic Science*, 16(4), 415–425. <https://doi.org/10.1017/S0954102004002238>
- Yuan, X. J., & Li, C. H. (2008). Climate modes in southern high latitudes and their impacts on Antarctic sea ice. *Journal of Geophysical Research*, 113(C6). <https://doi.org/10.1029/2006jc004067>

- Yuan, X. J., & Martinson, D. G. (2000). Antarctic sea ice extent variability and its global connectivity. *Journal of Climate*, 13(10), 1697–1717. [https://doi.org/10.1175/1520-0442\(2000\)013\(1697:Asieva\)2.0.Co;2](https://doi.org/10.1175/1520-0442(2000)013(1697:Asieva)2.0.Co;2)
- Yuan, X. J., & Martinson, D. G. (2001). The Antarctic dipole and its predictability. *Geophysical Research Letters*, 28(18), 3609–3612. <https://doi.org/10.1029/2001gl012969>
- Zhou, T. J., & Yu, R. C. (2004). Sea-surface temperature induced variability of the southern annular mode in an atmospheric general circulation model. *Geophysical Research Letters*, 31(24). <https://doi.org/10.1029/2004gl021473>